CRACKS FASTER THAN THE SHEAR WAVE SPEED

by

A.J. Rosakis
O. Samudrala
D. Coker

CALIFORNIA INSTITUTE OF TECHNOLOGY

PASADENA, CALIFORNIA

SM Report 98-17

CRACKS FASTER THAN THE SHEAR WAVE SPEED

by

A.J. Rosakis
O. Samudrala
D. Coker

December 1998

GRADUATE AERONAUTICAL LABORATORIES
CALIFORNIA INSTITUTE OF TECHNOLOGY
PASADENA, CA 91125

Cracks Faster than the Shear Wave Speed

A. J. Rosakis* O. Samudrala* D. Coker*

Abstract

Classical dynamic fracture theories predict the Rayleigh surface wave speed to be the limiting speed for propagation of in-plane cracks in homogeneous, linear-elastic materials subjected to remote loading. However, in the present study, experimental evidence to the contrary is reported, in which intersonic shear dominated crack growth is seen along weak planes in Homalite-100 under far-field asymmetric loading. It is seen that mode-II (in-plane shear) conditions are essential to attain intersonic crack-tip speeds. The stress field generated by the intersonically propagating crack-tip is recorded using photoelasticity and high speed photography. Intersonic shear cracks, featuring shear shock waves and large scale crack face frictional contact, are initially highly unstable and crack-tip speeds vary from the shear wave speed to the dilatational wave speed

*Graduate Aeronautical Laboratories, California Institute of Technology, CA 91125, USA

of the material. As steady state conditions are achieved, the mode-II intersonic cracks propagate at a constant speed of $\sqrt{2}c_s$. These observations have potential implications in geological settings where intersonic rupture velocities have been reported for crustal earthquakes.

Under remote loading conditions, the propagation speed (v) of an in-plane crack in a homogeneous, isotropic, linear-elastic material cannot exceed the Rayleigh wave speed (c_R) based on energetic considerations (1). However, experimentally observed crack-tip speeds seldom exceed $40 - 50\%$ of the Rayleigh wave speed even in the most brittle materials (2,3). A variety of explanations ranging from high strains (4) and micro damage zones around the crack-tip (3) to wavy crack paths (5) have been offered to reconcile the discrepancy between the observed terminal speed and the theoretically determined limit.

Washabaugh and Knauss (6) proposed that the observed maximal speed of crack propagation is inherently related to the strength of the material. On the basis of an earlier work by Ravichandar and Knauss (3), they argued that, in amorphous brittle solids a zone of microcracks is generated around a propagating crack-tip, which is responsible for significantly reducing the crack speed and eventually inducing crack-tip branching. In their experiments, they suppressed the formation of microcracks and the tendency for branching by fabricating weak planes along which cracks were

made to propagate under remote, symmetric opening (mode-I) loading conditions. Along these weak planes they reported mode-I subsonic (Speeds less than c_s) cracks asymptotically approaching the Rayleigh wave speed in the limit of vanishing bond strength. In a laboratory setting, the only experimental observations of crack-tip speeds greater than the shear wave speed, c_s, and less than the dilatational wave speed, c_l (intersonic), as well as speeds greater than c_l (supersonic) have been limited to cases where the loading is applied directly at the crack tip. Winkler *et.al.*, reported supersonic crack growth along weak crystallographic planes in anisotropic single crystals of potassium chloride, where the crack-tip was loaded by laser induced expanding plasma (7). At an entirely different length scale, indirect observations of intersonic shear rupture have been reported for shallow crustal earthquakes (8). Here the fault motion is primarily shear dominated and the material is not strictly monolithic since preferred weak rupture propagation paths exist in the form of fault lines.

Motivated by the observations of highly dynamic shear rupture during earthquakes, a substantial analytical effort has been made to model the mechanics of both subsonic and intersonic dynamic shear crack propagation. Andrews (9) performed a numerical investigation of a dynamically propagating shear crack with a slip weakening cohesive zone ahead of the tip. He observed that the terminal rupture velocity for a mode-II crack could be either less than the Rayleigh wave speed or slightly greater than $\sqrt{2}c_s$ depending on the cohesive strength of the fault plane ahead. Burridge

et.al., (10) performed an analytical investigation of the same problem and concluded that the velocity regime $c_s < v < \sqrt{2}c_s$ is inherently unstable, while the velocity regime $\sqrt{2}c_s < v < c_l$ is stable for intersonic shear crack propagation. Freund (11) obtained the asymptotic fields near a steady state mode-II intersonic crack which was prescribed to propagate along its own plane, in a homogeneous, isotropic, linear-elastic material. He concluded that $\sqrt{2}c_s$ is the only crack-tip speed for stable intersonic crack growth. Broberg (12) investigated the admissibility of various velocity regimes for mode-I and mode-II crack propagation along a prescribed straight line path, based on energy considerations. Since fracture is an inherently energy consuming process, he concluded that the velocity regimes in which the crack-tip energy release rate is negative are forbidden. Thus he ruled out the velocity regime $c_R < v < c_s$ for both mode-I and mode-II cracks, whereas the velocity regime $c_s < v < c_l$ was found to be forbidden for mode-I cracks only. In mode-II (in-plane shear), the velocity regime $c_s < v < c_l$ was found to be permissible according to the above stated criterion. However, up to now, no direct experimental confirmation of the admissibility of mode-II intersonic crack growth has been reported in the open literature.

Experimental Observations of Intersonic Crack Growth

Pursuant with the above observations, an experimental investigation was undertaken at Caltech to determine whether mode-II (in-plane shear) intersonic crack growth can be obtained in laboratory specimens under remote shear loading conditions. However, in monolithic, pre-notched laboratory specimens subjected to shear loading, it is invariably seen that after initiation from the notch tip the crack does not follow a straight path in line with the notch, but instead kinks in the local mode-I (symmetric opening) direction. To make mode-II crack growth possible, by suppressing kinking, and to simulate the prescribed path constraint of the analysis, we introduced a weak plane ahead of the notch tip in the form of a bond between two identical pieces of isotropic material. The bonding process was chosen carefully so that the mechanical properties of the bond are close to those of the bulk material. Thus we constructed a material system which, although not monolithic, can be considered homogeneous vis-a-vis its linear elastic constitutive description. However, fracture toughness along the bond line is lower, so that the material is inhomogeneous vis-a-vis its fracture properties. It may be worth noting here that the analytical continuum models discussed above, predicting an allowable crack speed regime for mode-II intersonic crack growth, are incapable of distinguishing between a homogeneous and monolithic material with no preferable crack path (weak bond) and a homogeneous

system involving a preferable crack path. The notion of inhomogeneity in fracture toughness is not contained in these continuum models which do not feature a fracture criterion.

Our experimental set-up used to investigate dynamic shear crack propagation under impact loading is shown in Fig. 1. Dynamic photoelasticity was chosen for capturing the stress field near the propagating crack-tip because of its ability to visualize shear shock waves anticipated by the intersonic crack solutions. Homalite-100, a brittle polyester resin which exhibits stress induced birefringence was chosen for this investigation. The specimens were made by bonding two identical 4 mm thick plates of Homalite as shown in Fig. 1. A polyester resin solution (99.5% by wt) was used for bonding, with methyl ethyl ketone peroxide as hardener (0.4%) and cobalt octate (0.1%) as catalyst. The bond was then cured for 48 hours at room temperature. The thickness of the bond was approximately $20 - 30\ \mu m$. A notch, 25 mm long and 2.3 mm wide, was machined on the upper half of the specimen along the bond line. A notch was chosen as the crack initiation site instead of a precrack to prevent the transmission of stress waves into the top half, thus ensuring that the notch tip is loaded under pure mode-II conditions. The relevant material properties of Homalite at a strain rate of $10^3 s^{-1}$ are : Young's modulus, $E = 5.3\ GPa$, Poisson's ratio, $\nu = 0.35$, plane stress longitudinal wave speed, $c_l = 2200\ m/s$ and shear wave speed, $c_s = 1255\ m/s$. In addition to the above described bonding procedure, a

limited number of specimens were bonded by the technique of temperature enhanced surface sintering as described by Washabaugh and Knauss (6). With this method there is no ambiguity regarding the constitutive homogeneity of the resulting bonded structure.

The specimen was subjected to asymmetric impact loading with a projectile as shown in Fig. 1. The projectile was 75mm long, 50mm in diameter and was made of hardened steel. A steel piece was bonded to the specimen at the impact site to prevent shattering and to induce a planar loading wave front. Typical impact velocities used in these experiments ranged from 25 to 35 m/s. The compressive longitudinal wave loads the notch-tip in a predominantly shear mode. The dynamic stress field produced by the loading was recorded using photoelasticity in conjunction with high speed photography. A coherent, monochromatic, plane-polarized, collimated laser beam of 50 mm diameter was transmitted through the specimen. The specimen was placed between two circular polarizers resulting in an isochromatic fringe pattern due to stress induced birefringence. Photoelasticity is a common optical technique used in solid mechanics applications which provides real time full field information and the reader is referred to Dally and Riley (13) for further details. The isochromatic fringe pattern is recorded by a rotating mirror type high-speed camera capable of recording 80 frames at framing rates up to 2 million frames per second. The laser used was an argon-ion laser operating at a wavelength of 514.5 nm in a pulsed mode of 8ns

pulse width. The generation of the isochromatic fringe patterns, which are contours of constant maximum in-plane shear stress, is governed by the stress optic law,

$$\frac{nF}{h} = 2\,\tau_{max} = \sigma_1 - \sigma_2 \tag{1}$$

where F is the material fringe constant, h is the thickness of the specimen, σ_1, σ_2 are the principal stresses and n is the isochromatic fringe order.

Fig. 2 shows a selected sequence of isochromatic fringe patterns around a shear crack as it initiates and propagates along the interface between two Homalite halves. The six frames included in the sequence are selected from two different experiments performed under identical conditions, except for the position of the field of view. The time after impact as well as the crack-tip speed is shown in each frame. In Fig. 2(A), the field of view encompasses the notch-tip elucidating the crack initiation process. The notch as well as the initial loading pulse are clearly visible in the first frame. The wave front is almost vertical, indicating that the notch is being subjected to predominantly mode-II loading. In the next frame we see the wave diffraction around the notch-tip and simultaneously observe the stress concentration building up. In the following frame we can discern a crack propagating dynamically along the interface after initiating from the notch-tip. In Fig. 2(B), the field of

view is located downstream from the notch-tip. In the first frame, we see a crack entering the field of view around which the shape of the isochromatic fringe pattern has changed drastically, and in the next frame we can clearly distinguish two lines radiating from the crack-tip across which the fringe pattern changes abruptly (lines of stress discontinuity). These two lines correspond to the two traveling shear shock waves, which limit the spread of shear waves emanating from the crack-tip as it propagates along the interface. The inclination of the shock waves indicates that the crack-tip has exceeded the shear wave speed of Homalite, and has become intersonic. The fringe pattern around the propagating crack in the last frame is very similar to that in the previous frame, indicating that the propagating crack has reached a steady state.

Typical crack-tip speed histories for two identical experiments varying only in the position of the field of view are shown in Fig. 3. Crack-tip speeds were determined using two methods. In the first method, a second order interpolating polynomial is obtained for every three successive points in the crack length history, which is then differentiated to give the crack velocity for the mid-point. In the second method, crack-tip speeds for frames in which the shock waves can be clearly distinguished, are obtained by measuring their angle of inclination to the crack faces. The angle of inclination β of the shock waves with the crack faces is related to crack-tip velocity through the relation,

$$v = \frac{c_s}{\sin \beta} \tag{2}$$

The variation of the crack-tip speed with crack length obtained using the first method is shown in Fig. 3(A), whereas that obtained by the second method is shown in 3(B). From Fig. 3 we see that the initially recorded crack-tip speed is close to the shear wave speed of Homalite (within experimental error of $\pm 100\ m/s$) beyond which it accelerates (at the order of $10^8\ ms^{-2}$), thus becoming intersonic. Thereafter, it continues to accelerate up to the plane stress dilatational wave speed of Homalite, following which it decelerates and ultimately reaches a steady state value of about $\sqrt{2}$ times the shear wave speed. As seen in Fig. 2, the shock wave angle under steady state conditions reaches an almost constant value around 45^o, corresponding to a crack-tip velocity of $\sqrt{2}c_s$. Note that the crack-tip velocity estimate from the shock wave angle is more accurate compared to that obtained from the crack length history due to the inherent propagation of errors in the differentiation process. It should be recalled here that the velocity regime between the Rayleigh wave speed and the shear wave speed is forbidden by theory based on energy considerations. For this velocity regime, the asymptotic solution predicts radiation of energy away from the crack-tip (negative energy release rate), which is not possible on physical grounds. Hence a crack with a smoothly varying velocity cannot pass through this forbidden regime.

According to this rationale, a crack will have to jump discontinuously from the sub-Rayleigh regime to the intersonic regime. However, another possibility for generating such intersonic speeds is to bypass this forbidden regime by nucleating a crack from the initial notch that instantaneously starts to propagate at a speed above c_s. Within our experimental time resolution the second scenario seems to be the most probable.

Mode-II Steady State Intersonic Crack Growth

Freund (11) obtained a steady state asymptotic solution for the stress and particle velocity fields near a mode-II crack intersonically propagating along a prescribed straight line path in a homogeneous, isotropic, linear-elastic material. According to this solution, the dominant term governing the stress state near the crack-tip is of the form (11,14),

$$\sigma_{ij}(\eta_1, \eta_2) = K_2^*(t) \left\{ \frac{f_{ij}(\theta_l, v)}{r_l^q} + \frac{g_{ij}(v)}{(-\eta_1 - \hat{\alpha}_s|\eta_2|)^q} H(-\eta_1 - \hat{\alpha}_s|\eta_2|) \right\} , \qquad (3)$$

where (η_1, η_2) are the coordinates of a point with respect to a moving coordinate system attached to the crack-tip, $f_{ij}(.,.)$ is a known function of crack-tip speed and angular position, $g_{ij}(.)$ is a function of crack-tip speed, $H(.)$ is the Heaviside step-function, and r_l, θ_l, α_l, and $\hat{\alpha}_s$, are defined as follows:

$$r_l = \sqrt{\eta_1^2 + \alpha_l^2 \eta_2^2}\ , \qquad \theta_l = tan^{-1} \frac{\alpha_l \eta_2}{\eta_1}\ , \tag{4}$$

$$\alpha_l = \sqrt{1 - v^2/c_l^2}\ , \qquad \hat{\alpha}_s = \sqrt{v^2/c_s^2 - 1}\ , \tag{5}$$

$K_2^*(t)$ is the intersonic stress intensity factor defined as

$$K_2^*(t) = \lim_{r \to 0} \sqrt{2\pi}\ r^q\ \sigma_{12}(r, 0)\ . \tag{6}$$

From Eqn. 3 we see that the asymptotic solution predicts two traveling waves of strong stress discontinuity attached to the crack-tip and inclined at $\beta = \tan^{-1}(1/\hat{\alpha}_s) = \sin^{-1}(c_s/v)$ to the crack faces (see argument of the Heaviside function). The stress field is singular at the crack-tip, and the singularity exponent q is a function of the crack-tip speed. Exponent q increases monotonically from 0 at $v = c_s$ to a value of $\frac{1}{2}$ at $v = \sqrt{2}c_s$ and there after decreases monotonically to 0 at $v = c_l$. An immediate implication of this behavior of the singularity exponent is that the dynamic crack-tip energy release rate is identically zero in the intersonic regime, except at $v = \sqrt{2}c_s$ where it has a finite value. However, fracture processes essentially involve breaking of bonds and creation of new surfaces, which requires a finite energy flow into the crack-tip. This explains the behavior of the crack-tip speed history in Fig. 3 where we

saw the propensity of an intersonic mode-II crack to propagate at a constant velocity of $\sqrt{2}c_s$ under steady state conditions. The stresses are also singular all along the lines of discontinuity with the same strength of singularity as that of the crack-tip. The crack-tip singularity is thus radiated away from the tip to create two *shear shock waves*. As one would expect, the existence of infinite stress jumps across these shock waves is not feasible and such a prediction is an artifact of the theory of linear elasticity. In real materials, however, this prediction corresponds very well with well-defined lines across which large but finite stress jumps occur. Fig. 4 compares an isochromatic fringe pattern recorded during the experiment (A) with that predicted by the theoretical solution (B). We can clearly distinguish two lines of finite width showing intense gradient of stress field emanating from the crack-tip. Both the experimental and simulated patterns are in good agreement with regard to the prediction of the two shock waves, their inclination to the crack faces as well as the oval shape of the fringes in front of the tip. However, the experimental fringe pattern is distorted by the stress field generated due to the loading pulse as well as due to crack face frictional contact and subsequent damage, as explained later. According to the linear elastic idealization these shear shocks are dissipation free (16,17). However, in real materials, shock waves are generally dissipative. Indeed, in most of the intersonic regime, where the energy flux directly into the crack-tip is zero, the only energy that is consumed is by the traveling shock waves at the tip vicinity. The pathology of

zero crack-tip energy release rate for an intersonic mode-II crack can be overcome simply by introducing a process zone of finite size ahead of the tip. When $v = \sqrt{2}c_s$, the energy release rate becomes finite and the $\sqrt{r}$ singularity reappears ($q = 0.5$). Only at this speed, the shock waves disappear, according to the theory, and there is no shock dissipation. The prediction of vanishing shock waves at $v = \sqrt{2}c_s$ was not observed in our experiments though the crack-tip appears to have reached a steady state. Part of the reason could be that the crack-tip is never truly propagating at exactly a steady state speed of $\sqrt{2}c_s$. Also, even after the crack-tip has reached a steady state, it takes a finite time for the shocks to detach from the crack-tip and vanish from the field of view.

Similar observations have been made with regard to intersonic motion of dislocations. Indeed, Eshelby (18) and Weertman (19) pointed out that radiation free intersonic motion of a glide dislocation in an isotropic solid is possible at a steady state speed of $\sqrt{2}c_s$. Weertman (19), in addition, showed that no such critical speed exists for a climb dislocation. Such a behavior can be expected from the fact that an intersonically propagating steady state mode-II crack can be considered as a superposition of a continuous array of glide dislocations, whereas an intersonically propagating steady state mode-I crack can be considered as a superposition of a continuous array of climb dislocations. A unified continuum approach treating both intersonic cracks and dislocations has been developed by Gao et.al. (20). More recently, Gumbsch and

Gao (21) have also have shown that dislocations can glide intersonically within the assumptions of discrete atomistic models.

Crack Face Contact Zone

An interesting experimental observation associated with intersonic crack propagation along a weak plane is shown in Fig. 5. This is a post-mortem photograph of the upper half of the test specimen showing an enlarged view of the area near the notch-tip. Starting from a finite distance ahead of the notch-tip along the crack path, a series of short opening cracks, parallel to each other can be observed. All the cracks have initiated on the upper crack-face, propagated a finite distance slightly off-vertical into the upper half of the specimen and subsequently got arrested. Occasionally, a few cracks have gone further. The angle of inclination of these cracks was measured to be approximately 11^o from the vertical $(\eta_2 - axis)$.

The initiation, propagation and arrest of these cracks can be observed "in vivo". Indeed, the high speed images of the isochromatic fringe pattern around the main shear crack-tip contain information about the initiation and the growth of these cracks. A typical photograph in which the phenomenon can be clearly distinguished is shown in Fig. 6. A series of symmetric shadow spots associated with the crack-tips

originate on the crack-face, propagate a finite distance into the upper half of the specimen and arrest subsequently. The centers of all these shadow spots fall on a single straight line inclined at about 23^o to the crack face. From this measure, as well as the small inclination of these cracks from the vertical, an estimate of their propagation speed is obtained to be $0.6c_s$. The symmetric nature of the shadow spots at these crack tips reveals the opening mode-I nature of these secondary cracks. Further evidence of their subsonic nature can be seen in the epicycloidal shape of the shadow spots surrounding their crack-tips. If we extend the line passing through the center of the shadow spots to the crack face, we can readily see that they originate a finite, albeit a small distance behind the main crack-tip. Hence, formation of these secondary cracks is not akin to the typical branching phenomenon observed in high speed subsonic crack propagation. These secondary, subsonic, opening mode cracks behind the main intersonic shear crack-tip cannot be explained completely based on the asymptotic solution for a traction free intersonic crack. The stress component σ_{11} (direct stress parallel to the crack faces) is tensile in the top half of the specimen, whereas it is compressive in the bottom half. This explains why the opening cracks are observed only in the tensile half of the specimen. If the cracks originated on a traction free surface, we would expect them to propagate vertically based on a maximum principal stress criterion for brittle fracture. The inclination of the secondary cracks from the vertical can only be explained in terms of a more complex state of

stress at the initiation site. It is conjectured that crack faces come into contact once the crack-tip exceeds the Rayleigh wave speed of the material. Evidence of this can be seen in Fig. 6, where a near vertical line of discontinuity emanating from the contact zone can be seen across which the fringe pattern changes abruptly. A similar phenomenon was observed during intersonic crack propagation along a bimaterial interface (17,22,23,24). Due to frictional sliding of the contact faces a two-dimensional state of stress exists at the crack faces along the contact zone (the secondary crack initiation site), which explains the 11^o inclination of the crack propagation path from the vertical. Assuming a linear frictional contact model ($\sigma_{12} = \lambda\sigma_{22}$), with a constant dynamic coefficient of friction λ, and further postulating that tensile failure will follow the predictions of the maximum principal stress fracture criterion, we can obtain bounds for λ. For a subsonic opening crack to propagate along the principal plane, the nature of the maximum principal stress should be tensile. A simple Mohr's circle analysis gives a lower bound for λ as 0.19. If we further assume that the stress component σ_{11} in the upper half of the specimen is tensile, the lower bound on λ is raised to 0.21. If in addition, $|\sigma_{11}| > |\sigma_{22}|$ then $\lambda > 0.4$. A precise estimate for λ can be obtained if a more elaborate model of intersonic shear crack growth, which includes crack face frictional contact, is developed (31).

Concluding Remarks

To the authors' knowledge, this article describes the first experimental observation of shear-dominated intersonic crack growth. We saw that intersonic crack propagation is possible along a weak plane in a homogeneous material (homogeneous with respect to its constitutive properties) subjected to far-field mode-II (in-plane shear) loading conditions. The lower fracture toughness along the weak plane makes it a preferred path for crack propagation by suppressing kinking and branching, thus ensuring that the crack propagates under mode-II conditions. However, in a purely homogeneous material (homogeneous with respect to both constitutive and fracture properties) with no preferred paths for crack propagation, a mode-II crack immediately after initiation, kinks in the local direction of maximum energy release rate which is nearly coincident with the local mode-I direction (25). The competition between kinking, in a locally opening mode, and straight-ahead propagation, in a primarily shear mode, can be biased towards a shear, straight-ahead propagation by artificially reducing the fracture toughness along the preferred path. Moreover, mode-II conditions near a propagating crack-tip are found to be necessary in achieving intersonic crack-tip speeds. Washabaugh and Knauss (6) in their mode-I (opening) experiments observed that no matter how weak the crack propagation path is, a mode-I crack never exceeds the Rayleigh wave speed of the material. This observation is supported by the

asymptotic solution, which predicts a radiation of energy (negative unbounded energy release rate) away from the crack-tip during mode-I intersonic crack propagation (12), thus excluding this crack growth scenario. However, intersonic shear cracks are found to theoretically have a non-negative energy release rate thus allowing the possibility of intersonic mode-II growth as confirmed experimentally in this article.

Dynamic shear crack propagation is of primary interest in modeling earthquake source dynamics. Analysis of far-field wave forms generated by shallow crustal earthquakes indicates that the source process represents a sudden stress drop across a rupture front, similar to a crack. Furthermore, the high pressures and temperatures deep inside the earth's crust rule out the existence of tensile cracks, allowing for shear cracks only (26,27). Average rupture velocities inferred for most of the shallow crustal earthquakes observed so far range from 0.7 to 0.9 c_s. Rupture propagation is very sensitive to the properties of the surrounding material and as such is a highly transient process. For average rupture velocities close to the shear wave speed, it is plausible that locally, for short durations, rupture velocities could be intersonic (31). Archuleta (8) suggested intersonic rupture velocities based on his analysis of the strong motion data recorded during the 1979 Imperial valley earthquake. Moreover, numerical studies on propagation of in-plane shear cracks by Das and Aki (28) as well as Andrews (9) have shown that depending on the strength of the fault plane, propagation speeds can be either sub-Rayleigh or intersonic. Indeed our current ex-

periments have convincingly shown that intersonic rupture velocities are possible for shear cracks propagating along a weak plane.

In an analogous situation, cracks along interfaces in bimaterials composed of solids with strong wave speed mismatch have been observed to propagate at speeds that are intersonic with respect to the solid that has the lower wave speeds (16,17). However, such cracks were never observed to become intersonic with respect to both solids. Again in this case, interfacial cracks initiated under predominantly shear loading reached intersonic speeds. Here, the bimaterial bond (irrespective of its strength) acts as a preferred crack propagation direction. Crack face contact zones were also observed along bimaterial interfaces during intersonic crack propagation (29). In yet another material system which exhibits preferred crack propagation directions, intersonic crack growth was observed in unidirectional fiber-reinforced composites under shear dominated loading conditions (30,15). Here again, the fiber/matrix interface provides a weak plane which facilitates shear dominated crack propagation.

To summarize, the essential requirement for intersonic crack growth is the existence of mode-II conditions near the propagating crack-tip. One way to ensure that a propagating crack-tip remains under mode-II conditions is to introduce a weak plane along the preferred crack path. Under such circumstances, a mode-II crack, immediately after initiation, can start to propagate at intersonic speeds and when it does

so, it features the formation of shear shock waves emitted from the propagating shear crack tip and large scale crack face frictional contact.

References and Notes

1. L. B. Freund, *Dynamic Fracture Mechanics* (Cambridge Univ. Press, 1990).

2. B. Cotterell, *Appl. Mat. Res.*, **4**, 227 (1965).

3. K. Ravichandar and W. G. Knauss, *Int. J. Fract.*, **26**, 141 (1984).

4. K. B. Broberg, *J. Appl. Mech.*, **31**, 546 (1964).

5. H. Gao, *J. Mech. Phys. Solids*, **1**, 457 (1993).

6. P. D. Washabaugh and W. G. Knauss, *Int. J. Fract.*, **65**, 97 (1994).

7. S. Winkler, D. R. Curran and D. A. Shockey, *Int. J. Fract.*, **6**, 151, 271 (1970).

8. R. J. Archuleta, *Bull. Seis. Soc. Am.*, **70**, 671 (1980).

9. D. J. Andrews, *J. Geophys. Res.*, **81**, 3575 (1976).

10. R. Burridge, G. Conn and L. B. Freund, *J. Geophys. Res.* **84**, 2210 (1979).

11. L. B. Freund, *J. Geophys. Res.*, **84**, B5, 2199 (1979).

12. K. B. Broberg, *Int. J. Fract.*, **39**, 1 (1989).

13. J. W. Dally and W. F. Riley, *Experimental Stress Analysis*, (McGraw-Hill, 1991).

14. There is a typographical error in the expression for $g_{ij}(v)$ and q as given in (11). The correct expression can be deduced from the orthotropic solution given in (15).

15. Y. Huang, W. Wang, C. Liu and A. J. Rosakis, to appear in *J. Mech. Phys. Solids*, (1998).

16. R. Abeyaratne and J. K. Knowles, *J. Mech. Phys. Solids*, **38**, 345 (1990).

17. C. Liu, Y. Huang, and A. J. Rosakis, *J. Mech. Phys. Solids*, **43**, 189 (1995).

18. J. D. Eshelby, *Proc. Roy. Soc. Lond.*, **62A**, 307 (1949).

19. J. Weertman, *in Mathematical Theory of Dislocations*, ed. T. Mura, ASME, New York, 178 (1969).

20. H. Gao, Y. Huang, P. Gumbsch, and A. J. Rosakis, *to appear in J. Mech. Phys. Solids* (1998).

21. P. Gumbsch and H. Gao, *submitted for publication in Science*, (1998).

22. J. Lambros and A. J. Rosakis, *J. Mech. Phys. Solids*, **43**, 169 (1995)

23. R. P. Singh, J. Lambros, A. Shukla, and A. J. Rosakis, *Proc. R. Soc. Lond.*, **453A**, 2649 (1997).

24. A. Needleman and A. J. Rosakis, *to appear in J. Mech. Phys. Solids.*, (1998).

25. J. W. Hutchinson and Z. Suo, *Adv. Appl. Mech.*, **29**, 63, (1992).

26. J. R. Rice, *in Physics of Earth's Interior*, E. Boschi, Ed. (Amsterdam, 1980), pp.555-649.

27. R. Dmowska and J. R. Rice, *in Continuum Theories in Solid Earth Physics*, R. Teisseyre, Ed. (Elsevier, 1986), pp.187-255.

28. S. Das and K. Aki, *Geophys. J. R. Astron. Soc.*, **50**, 643, (1977).

29. O. Samudrala and A. J. Rosakis, *Caltech SM Report* (1998).

30. D. Coker and A. J. Rosakis, *Caltech SM Report # 98-16* (1998).

31. A. J. Rosakis would also like to thank Prof. J. R. Rice of Harvard University for penetrating discussions during his November 1998 visit to Harvard.

32. The authors would like to acknowledge the support of the National Science Foundation (Grant # CMS9424113) and the Office of Naval Research (Grant # N00014-95-0453).

List of Figures

from the contact zone. (**B**) Schematic showing the initiation and propagation of the tensile secondary cracks and the 2-D stress state on the contact face.

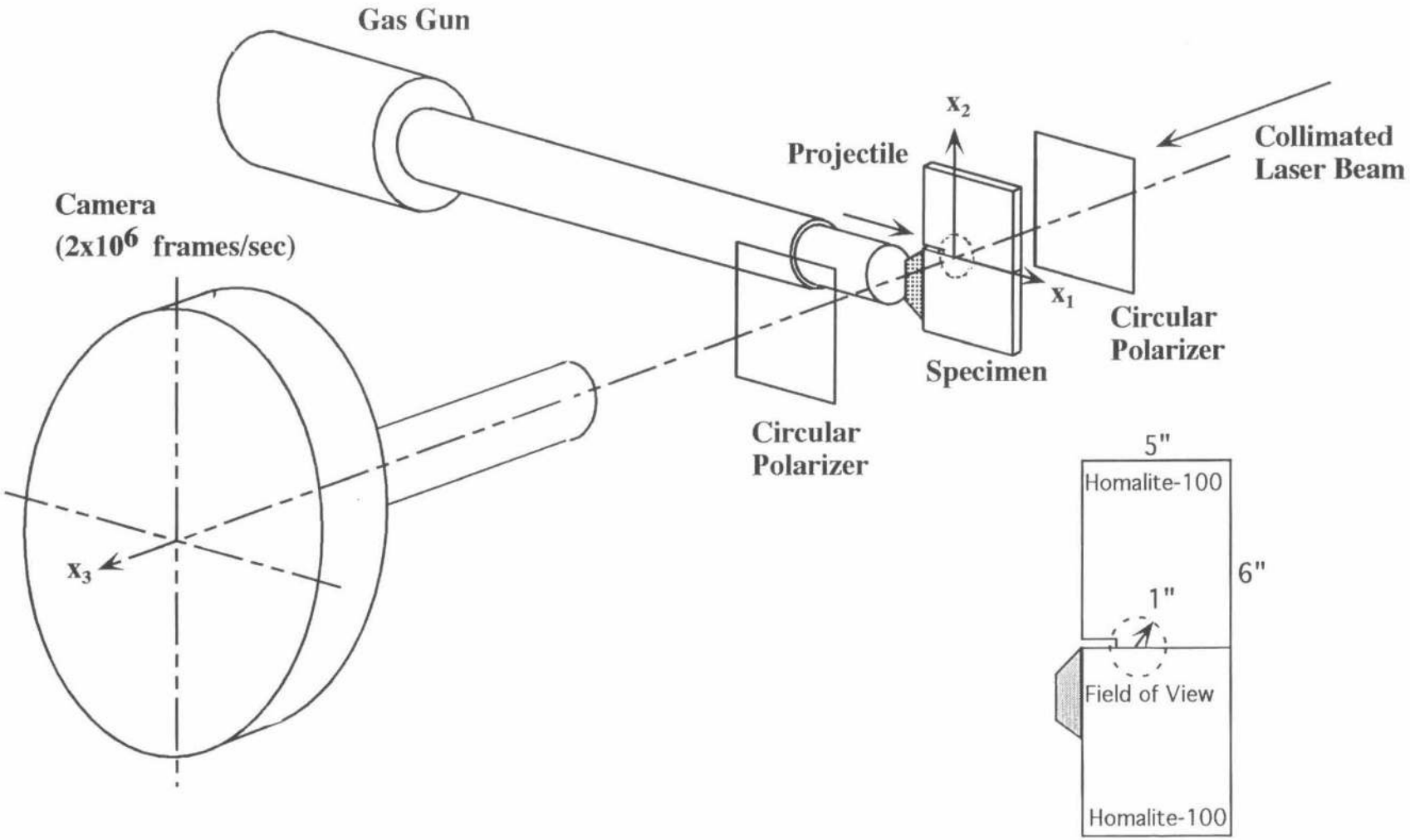
Gas Gun
Camera
(2x10^6 frames/sec)
Projectile
x2
x1
Collimated
Laser Beam
Circular
Polarizer
Specimen
Circular
Polarizer
x3
5"
Homalite-100
6"
1"
Field of View
Homalite-100

Fig. 1

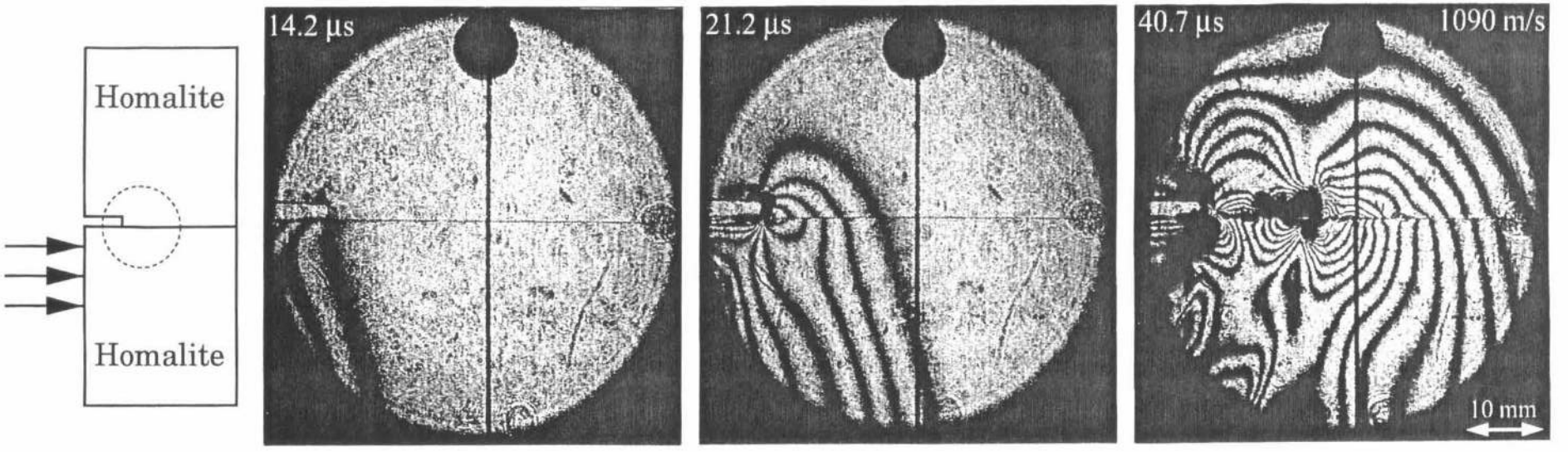
Homalite
Homalite
14.2 µs
21.2 µs
40.7 µs
1090 m/s
10 mm

(A)

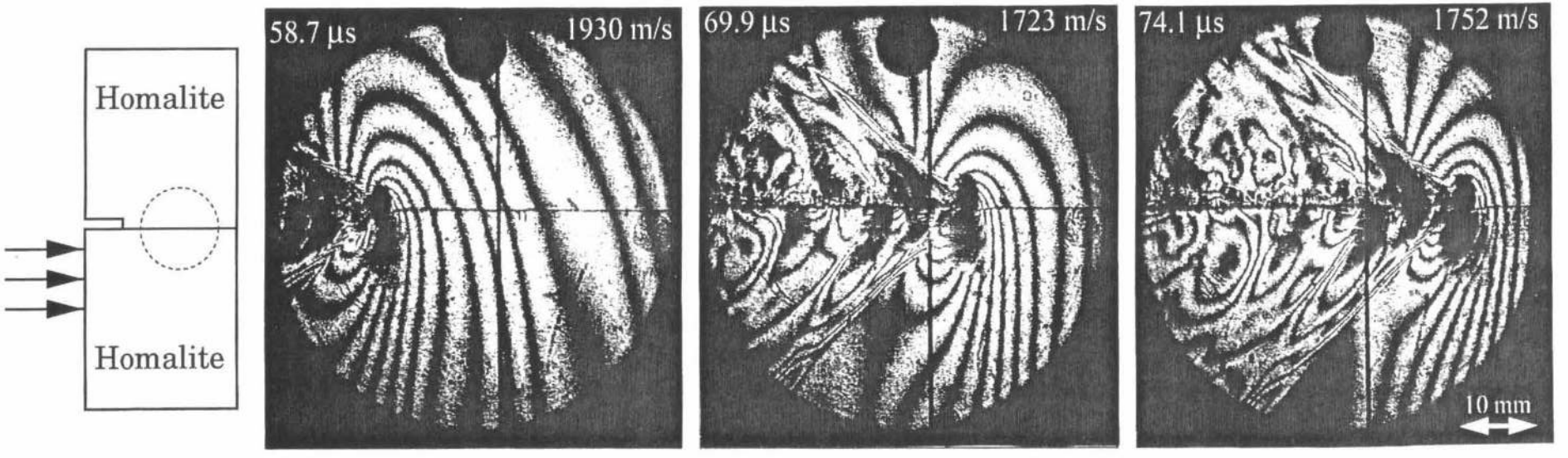
Homalite
Homalite
58.7 µs
1930 m/s
69.9 µs
1723 m/s
74.1 µs
1752 m/s
10 mm

(B)

Fig. 2

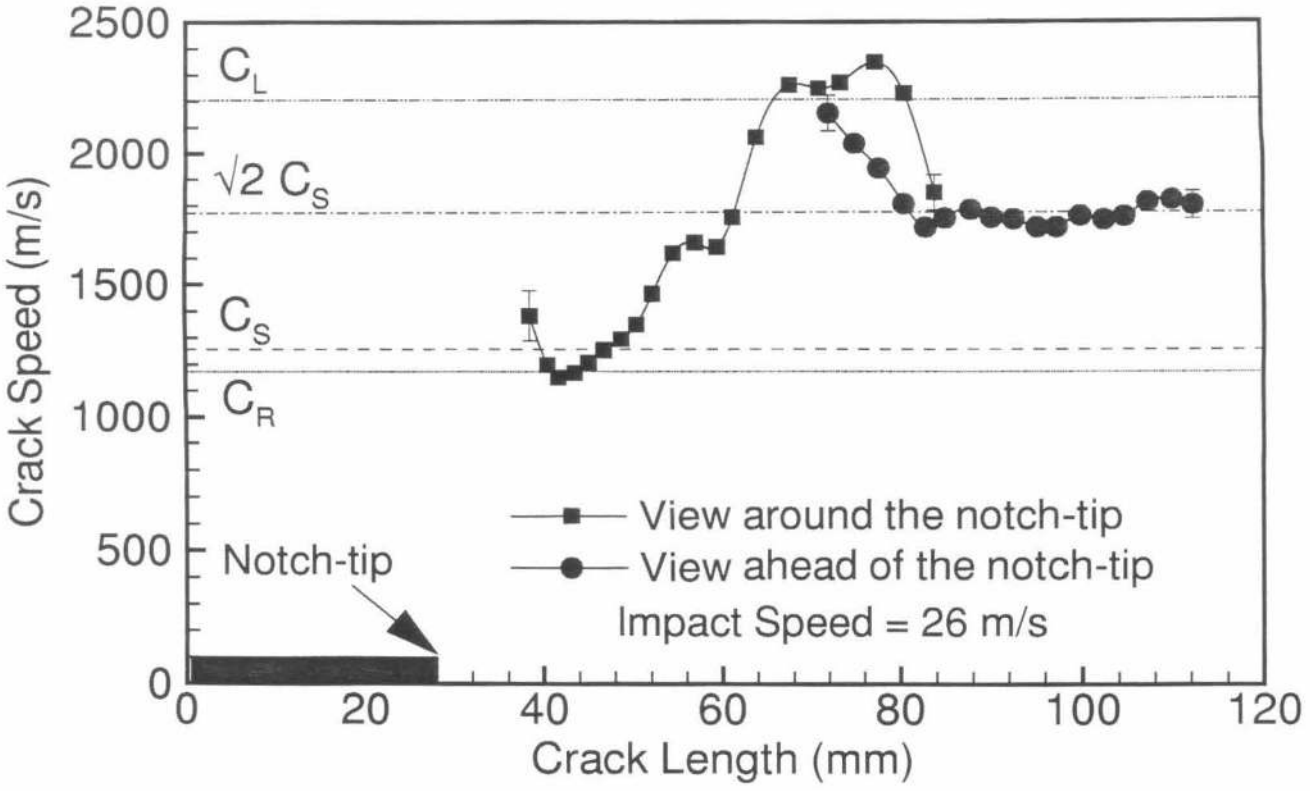
2500
2000
1500
1000
500
0
Crack Speed (m/s)
C_L
$\sqrt{2}\ C_S$
C_S
C_R
Notch-tip
View around the notch-tip
View ahead of the notch-tip
Impact Speed = 26 m/s
0
20
40
60
80
100
120
Crack Length (mm)

(A)

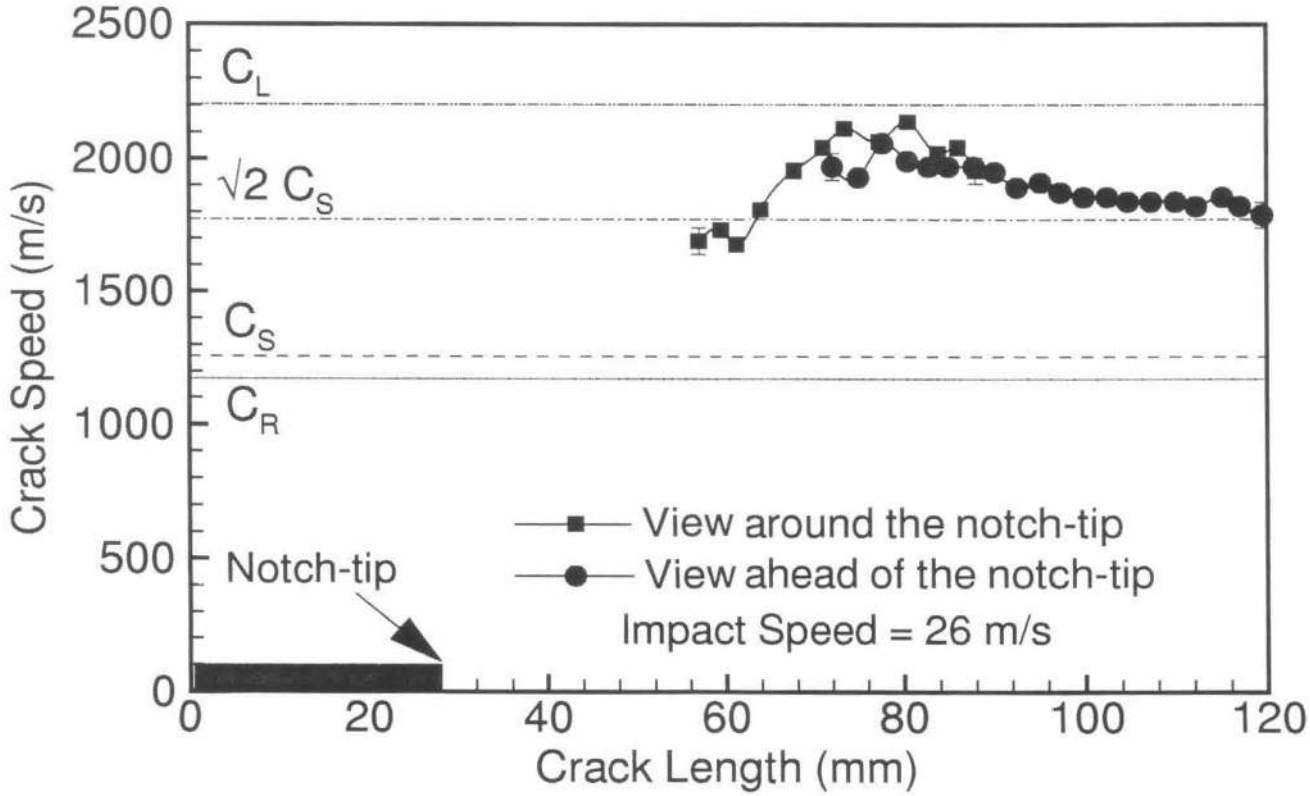
2500
2000
1500
1000
500
0
Crack Speed (m/s)
C_L
$\sqrt{2}\ C_S$
C_S
C_R
Notch-tip
View around the notch-tip
View ahead of the notch-tip
Impact Speed = 26 m/s
0
20
40
60
80
100
120
Crack Length (mm)

(B)

Fig. 3

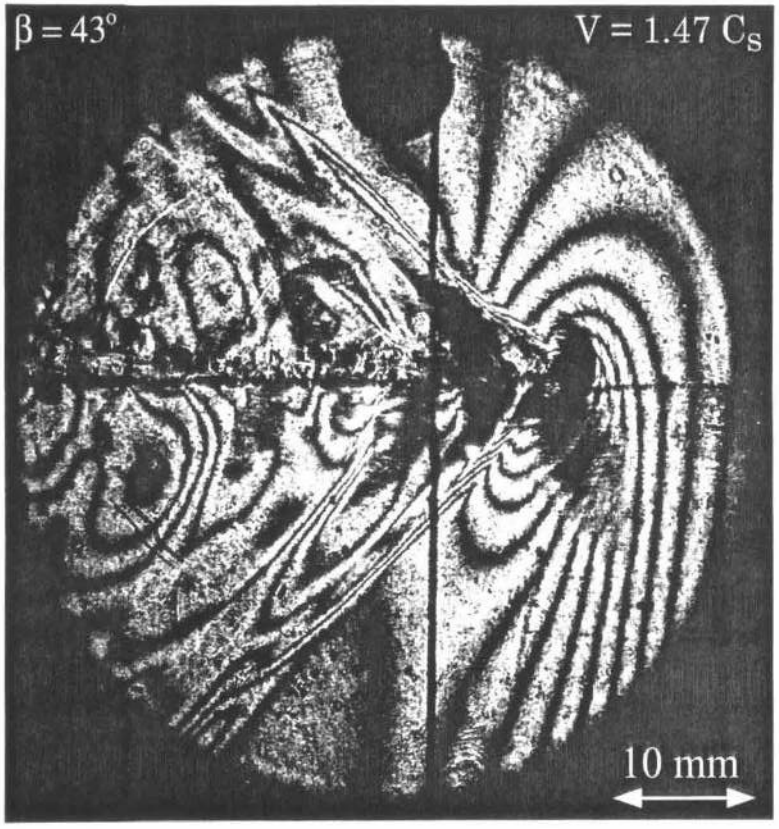

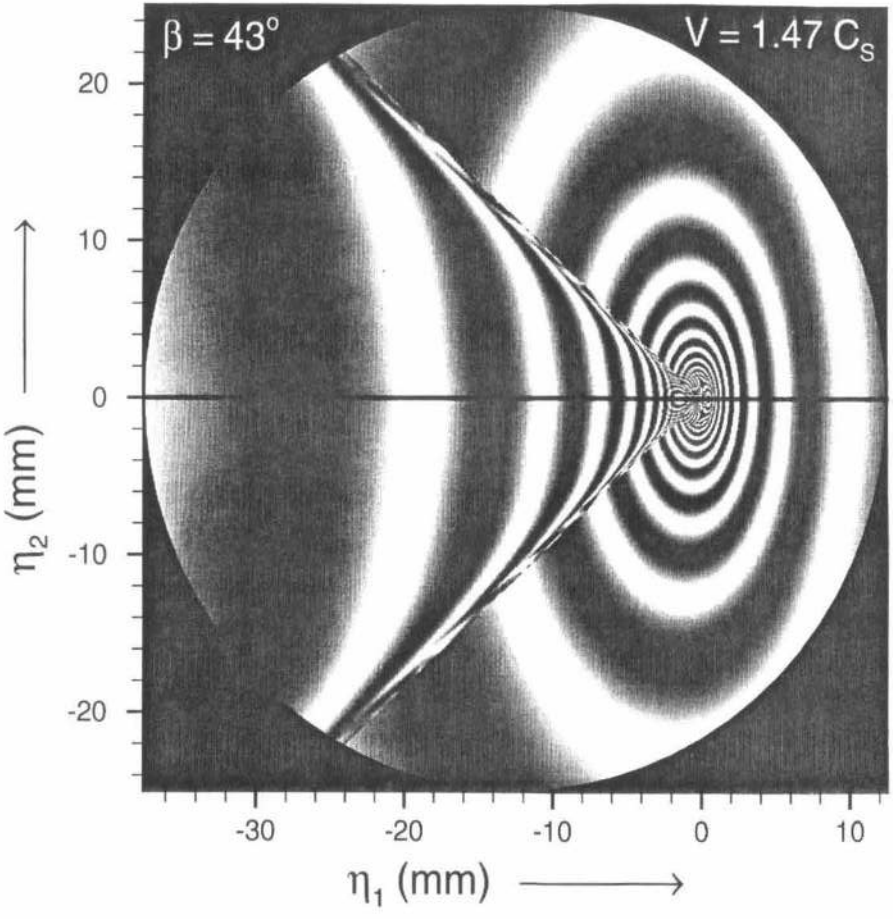

(A) (B)

Fig. 4

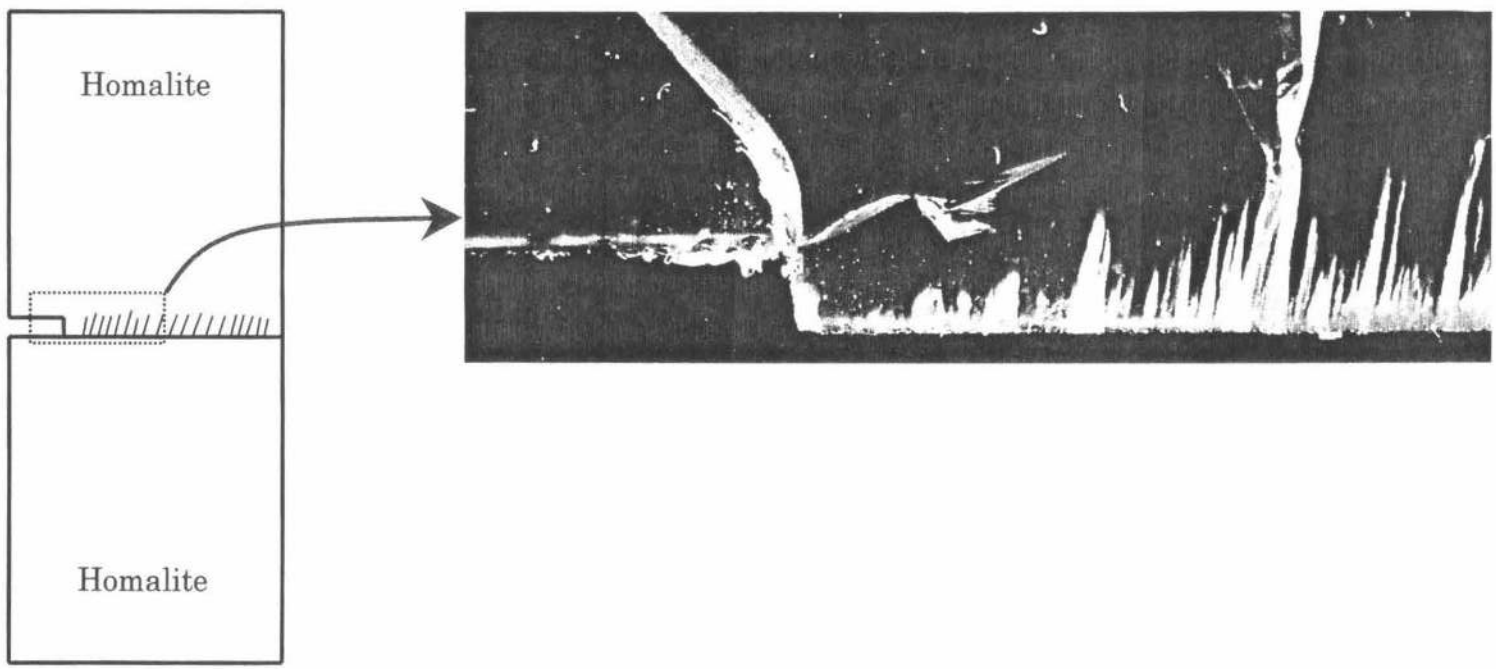

Fig. 5

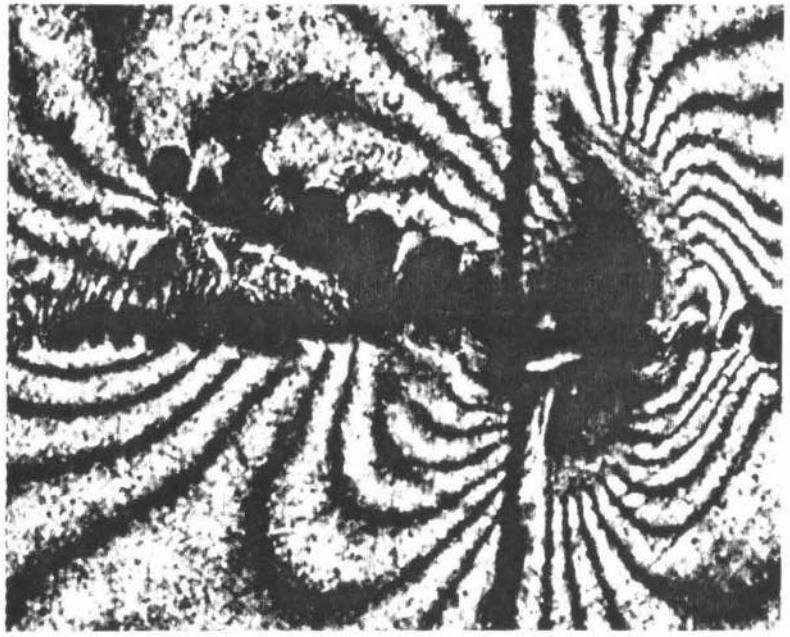

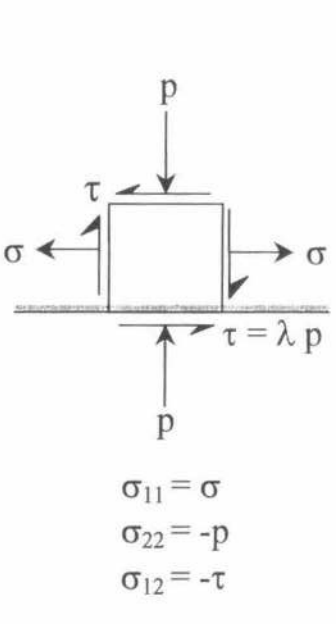

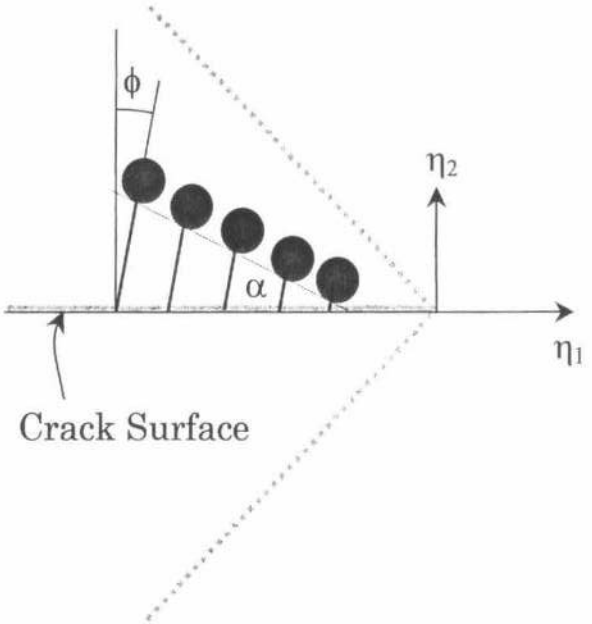

(A)

(B)

Fig. 6